

Contents list available at CBIORE journal website

International Journal of Renewable Energy Development

Journal homepage: https://ijred.cbiore.id



Research Article

Batch and fixed-bed adsorption of phosphate and nitrate on char derived by the co-pyrolysis of waste tires and corn cobs

Sally Ali Hussein* o and Muthanna Jabar Ahmedo

Department of Chemical Engineering, College of Engineering, University of Baghdad, Iraq

Abstract. The existence of both phosphorus (P) and nitrogen (N) in water can severely affect the aquatic environment by causing eutrophication phenomena. Co-pyrolysis has emerged as a viable thermal technology for converting various solid waste blends into extremely effective char. In this research, the co-pyrolysis of waste tires (WT) and corn cobs (CC) into char and its application as an adsorbent against nitrate and phosphate were investigated. The influence of various variables, including WT/CC blend composition, pyrolysis time, and pyrolysis temperature, on the performance and yield of char was also considered using batch and fixed-bed column tests. The characteristics of the obtained char were evaluated through Brunauer-Emmett-Teller analysis, Fourier transform infrared, and Field emission scanning electron microscopy with energy-dispersive X-ray analysis. Enhanced functioning and adsorption of pollutants were seen in the resulting material when the blend mixture was 25% WT + 75% CC. From the Sips isotherm, which exhibited high R² values (0.9957, 0.9953) as compared to the Langmuir and the Freundlich isotherms, the maximum adsorption capacities of nitrate and phosphate were 59.19 and 77.23 mg/g, respectively. Two models, one for pseudo-second order and one for pseudo-first order, were used to examine the kinetic data, showing a strong adherence to the former model for the studied pollutants. Also, two popular fixed-bed adsorption models, the Yoon-Nelson and Thomas models, were utilized to match the adsorption data. Under varying circumstances, the findings agreed with the Yoon-Nelson and Thomas models, as measured by the correlation coefficient R² values (0.8853-0.9946) for phosphate, (0.9463-0.9913) for nitrate, and (0.9658-0.9965) for phosphate, (0.8848-0.9966) for nitrate, respectively.

Keywords: Co-pyrolysis, Waste blend, Anionic pollutants, Binary adsorption, Fixed bed.



@ The author(s). Published by CBIORE. This is an open-access article under the CC BY-SA license (http://creativecommons.org/licenses/by-sa/4.0/).

Received: 1st August 2025; Revised: 18th Oct 2025; Accepted: 29th Oct 2025; Available online: 2nd Nov 2025

1. Introduction

The adverse effects on the natural environment, particularly water quality, have long been linked to natural and human Folch, progress (Salgot and However, nowadays, water contamination is thought of as a big issue all around the world. Even though water makes up about 70% of the Earth's surface, the biggest problem on the global level is the accessibility of fresh water. The increasing demand for freshwater is burdening already scarce wastewater treatment facilities. All living things, including humans, rely on clean water for survival (Huong et al., 2019; dos Santos et al., 2025). Phosphate, Nitrate, poisonous metalloids, heavy metal ions, and synthetic organic compounds are among the inorganic and organic pollutants that can be released into water, leading to water contamination (Braun et al., 2019; Liu, Shen and Qi, 2019; Hasan, Mohd Saharuddin and Muhamad, 2025). An abundance of agricultural growth nutrients, phosphate, and nitrogen in the water surface leads to algal bloom, subsequently leading to eutrophication issues. Eutrophication, or the overfertilization of water bodies, is a growing concern. Alterations to the aquatic ecosystem's species composition, toxic algal blooms, or hypoxia at the water's surface resulted from this occurrence. This poses a significant challenge for various waterrelated applications (Boeykens et al., 2017; Cheng et al., 2021). Numerous environmental regulatory agencies, including the United States Environmental Protection Agency (USEPA), have

adopted regulations that limit pollutant levels for nitrates at 10 mg/L and phosphate maximum concentrations of 50 ug/L for use in drinking water (Awual et al., 2011; Fatima et al., 2021). Rising NO₃-1 concentrations in drinking water negatively impact human health beyond eutrophication, particularly in newborns (blue baby syndrome being a specific example)(Ahmed, Hameed and Khan, 2023; Wang, Amano and Machida, 2024) . Phosphate is toxic to human organs and causes dyspnea in children exposed to concentrations of 230 mg/L, according to evidence (Kang and Jeen, 2021). Thus, before discharging treated wastewater into the bodies of water, it is crucial to extract the phosphate and nitrate from wastewater or other contaminated sources and transfer their concentration to a level that complies with the effluent's standard criteria (Priya et al., 2022). Consequently, environmental scientists are focusing much of their attention on finding better ways to treat water for nitrogen and phosphorus. Many researchers have recently started looking into this issue. Consequently, there is an immediate need to create treatment technologies that are both highly efficient and inexpensive for the removal of PO₄-3 and NO₃-1 from wastewater (Han et al., 2022). There are several methods available for treating wastewater to eliminate phosphate and nitrate. In general, they comprise chemical precipitation (Uludag-Demirer and Othman, 2009), reverse osmosis (Häyrynen et al., 2008), biological processes (De-Bashan et al., 2002), coagulation-flocculation(Wang et al., 2011),

* Corresponding author

and adsorption (Abdul Wahab, Soaded Alsaqqar and Kareem Ali, 2011; Mohammed and Rashid, 2012; Baboli and Bafkar, 2023; Jamka and Mohammed, 2023; Jamka *et al.*, 2023).

Adsorption is a suitable technology for purifying water among the several available processes because of its efficient, economical, and ecologically friendly operation. It was possible to purify water and manage waste streams simultaneously by using adsorbents made from various waste sources to remove contaminants from water (Ghalandari, Hashemipour and Bagheri, 2020; Khanday et al., 2025). Char applications for nutrient adsorption have recently garnered increased interest(Konneh et al., 2021). Char, which is made from organic materials by pyrolysis, resembles charcoal. Due to its aromatic nature, char outperforms the initial feedstock and exhibits chemical and biological stability. Chars' properties and surface chemistry were reportedly affected by the feedstock and operational pyrolysis parameters (composite material, retention time, and pyrolysis temperature) (Alsewaileh, Usman and Al-Wabel, 2019; Mohamed and J. Ahmed, 2019), Biomass chars' chemical and structural features significantly influence the overall reaction kinetics and conversion behavior(Eisenbach et al., 2025).

Agricultural waste is regarded as a significant precursor to its affordability, renewability, safety, abundant availability, and accessibility; furthermore, it possesses high carbon content and low ash level (Ahmed and Dhedan, 2012). Recently, corn has emerged as the preeminent crop globally, with maize grain utilized for food, feed, and industrial raw materials. A substantial quantity of corn cobs was produced from the initial corn grain by mass(Nguyen et al., 2022). Moreover, the disposal of waste tires is a worldwide problem. Annually, around 330 million trash tires are discarded globally. Waste tires are often disposed of in landfills, which pose significant dangers related to biological and chemical resistance to decomposition and mineral leaching. Energy recovery through thermal valorization is a favored approach for scrap tire disposal. Thermal valorization methods for waste tires include pyrolysis, combustion, and gasification(Issac, Dai and Zhang, 2019; Betancur et al., 2020).

The process of pyrolysis has evolved into a practical method for recycling garbage. The useful byproducts, such as pyrolytic carbon black, gas, and oil, can be extracted using pyrolysis, a thermal breakdown process in an inert environment. The process of pyrolysis, which involves the extraction of valuable

materials from garbage, offers a sustainable alternative to traditional recycling methods that result in toxic emissions or lengthy disposal (Abd and Al-Yaqoobi, 2023; Singh Yadav *et al.*, 2023; Abd, Al-yaqoobi and Abdul-Majeed, 2024; Ramani *et al.*, 2025). This study investigates the synergistic effect of blend waste during co-pyrolysis, the influence of their blending ratios on the char produced, and the char's capacity to adsorb nutrients from water. Theoretically, a framework for the broad and large-scale use of waste tires and biomass-derived char can be built, thus benefiting both parties. Additionally, the kinetic and isothermal models in the batch adsorption process and the breakthrough curves in continuous adsorption were examined.

2. Materials and Procedures

2.1 Materials

This project utilized locally produced raw corn cobs (CC) and scrip tires (WT) from Baghdad, Iraq. The first step was to dehydrate WT and CC in a preheated oven at 100 °C and 80 °C for 12 hours, respectively, after being rinsed multiple times with distilled water. Crushed to a size of (2 mm - 1.7 mm) for later use, the dehydrated WT and CC were saved. Thomas Baker of India supplied purities of 99% and 98% KNO $_3$ and KH $_2$ PO $_4$, while conc. HCl and NaOH were sourced from Himedia of India, respectively, and were utilized in this investigation.

2.2 Preparation of Char

Crushed CC was mixed with WT in varying weight-to-weight ratios and then heated to pyrolysis to yield char, as illustrated in Figure 1. A stainless-steel reactor with a 2.5 cm inside diameter and a 10 cm height was used to hold the combined sample. The pyrolysis gases could escape through a 1.5 mm hole in the center of the removable lid at one end of the reactor, while the other end was sealed. The reactor, a Nabertherm N-20/H from Germany, was heated in a furnace operating at an even rate of 10 °C/min for a range of durations (60 min to 180 min) and temperatures (400 - 900 °C). The char sample was removed from the furnace and allowed to cool to ambient temperatures after undergoing pyrolysis under the given conditions. At the studied mixing ratios, the char samples from CC and WT blends were 100% WT+0 % CC, 75% WT+25 % CC, 50% WT+50 % CC, 25% WT+75 % CC, and 0% WT+100 % CC, in that order. The char samples were repeatedly cleaned with distilled water



Fig. 1. Schematic diagram for char preparation

before being dehydrated and ready for ultimate utilization. We calculated the char yield by using this method:

$$Yield \% = \frac{Wf}{Wo} * 100 \tag{1}$$

Where W_f is the final char product weight in grams and W_o is the weight of the dry WT, CC, or their blends (g), respectively.

2.3 Characterization of Char

The chars derived from WT, CC, and combinations of the two were analyzed using a range of methodologies. The KBr pellet method was used with a Bruker Vector 22 spectrometer to capture the materials' Infrared Fourier transform (FTIR) spectra in the 500-4000 cm⁻¹ range. The morphology of the char was identified using field emission scanning electron microscopy (FE-SEM). All of the samples were coated with gold. An FE-SEM Zeiss equipped with a BRUKER EDX system performed energydispersive X-ray (EDX) analysis. The EDX technology elemental randoms were carried out at randomly selected areas of the sample to determine the distribution of atoms on the surface. Using the Brunauer-Emmett-Teller (BET) technique, the surface area was measured using the micrometric ASAP 2020 instrument. The char's surface charge zeta potential was calculated using the zeta potential instrument (Brookhaven, 2013, USA).

2.4 Adsorption Experiment

Solution stocks of PO₄-3 and NO₃-1 were prepared using KNO₃ and KH₂PO₄, with a 1000 mg/L concentration range. The stock solution was used to dilute the following adsorption solutions, which ranged in concentration from 100 to 700 mg/L. Batch experiments were used to determine the adsorption capabilities of different chars for PO4-3 and NO3-1. 0.1 g of each char sample was added to 50 mL of a solution containing 100 and 700 mg/L of PO₄-3 and NO₃-1, respectively. The pH was brought down to 2 using drops of 0.1 M HCl. The 50 mL Erlenmeyer containers were filled with the mixture and left at room temperature. A tiny membrane filter (0.45 µm) separated the char and adsorption solution after 24 hours. This was followed by synthesizing the remaining PO4-3 and NO3-1 amounts using ion chromatography (IC). A formula was used to compute the equilibrium adsorption amount of PO4-3 and NO3-1, denoted as qe (mg/g):

$$q_e = \frac{(C_o - C_e) V}{W} \tag{2}$$

 C_e and C_o (mg/L) are the concentrations of NO_3^{-1} and PO_4^{-3} solutions at initial and saturation, respectively. W (g) is the char weight used, and V (L) is the solution volume.

2.5 Adsorption Isotherm

Adsorption isotherms can characterize any system's adsorbate-adsorbent interaction. Gathering the parameters from isothermal data modelling was necessary to construct and analyze the adsorption systems correctly. Three distinct isotherm models were employed to ascertain the maximal adsorption capacity. The Langmuir equation states that the adsorbate has a monolayer-free molecular distribution attached to a homogeneous surface. Two popular empirical models are the Freundlich and Langmuir-Freundlich models, which are used to understand adsorption on heterogeneous surfaces.

Langmuir model:
$$q_e = \frac{q_m k_1 c_e}{1 + k_1 c_e}$$
 (3)

Freundlich model:
$$q_e = k_f c_e^{1/n}$$
 (4)

Langmuir-Freundlich model:
$$q_e = \frac{q_s k c_e^{1/m}}{1 + k c_e^{1/m}}$$
 (5)

Where q_m (mg/g) is the maximum amount of (PO₄-3 and NO₃-1) adsorbed per unit mass of char, In a solution, Ce (mg/l) represents the adsorbate concentration at adsorption equilibrium; the constants of the associated isotherm models are denoted by k_l (l/mg), k_f ((mg (l-1/n)-l1/n)/g), and k (l1/m.mg-1/m), respectively, the index denoting heterogeneity is n or m.

2.6 Adsorption Kinetics

The adsorption of PO₄-3 and NO₃-1 on char was determined using two standard adsorption models: pseudo-first order and pseudo-second order.

Pseudo-first-order model:
$$q_t = q_e(1 - e^{-k_1 t})$$
 (6)

Pseudo-second order model:
$$q_t = \frac{k_2 q_e^2}{(1+k_2 q_e t)}$$
 (7)

Where the quantity of adsorbate adsorbed by char on each gram at the adsorption equilibrium and at any given time is denoted by q_e and q_t (mg/g), respectively; the related rate constants of the two kinetic models are denoted by k_1 (hr⁻¹) and k_2 (g·mg⁻¹·hr⁻¹)

2.7 Fixed Bed Column Experiments

Figure 2 illustrates that the fixed-bed column consists of a Pyrex glass tube measuring 39.5 cm in height, 17.6 mm in outer diameter, and 14 mm in inner diameter. A single layer of substance tightly arranged around a stainless-steel sieve was attached to the column's base. The required bed level of the adsorbent was achieved by adding a specific amount of the produced char to the column, which might be 5, 10, or 15 cm (corresponding to 1.7765, 3.4827, and 4.9293 g of char, respectively). Subsequently, support was provided to the columns to ensure a uniform flow of the solution. A dosing pump was used to adjust the flow rate of a binary NO₃⁻¹/PO₄⁻³ solution at 5, 10, and 15 mL/min while pumped upstream through the (WATSON-MARLOW LIMITED/ column **FLAMOUTH** CORNWELL ENGLAND). The concentrations of the solution were 100, 300, and 600 ppm. Ion chromatography (IC) (Cecil, 2014) was used to measure the concentration of a binary NO₃

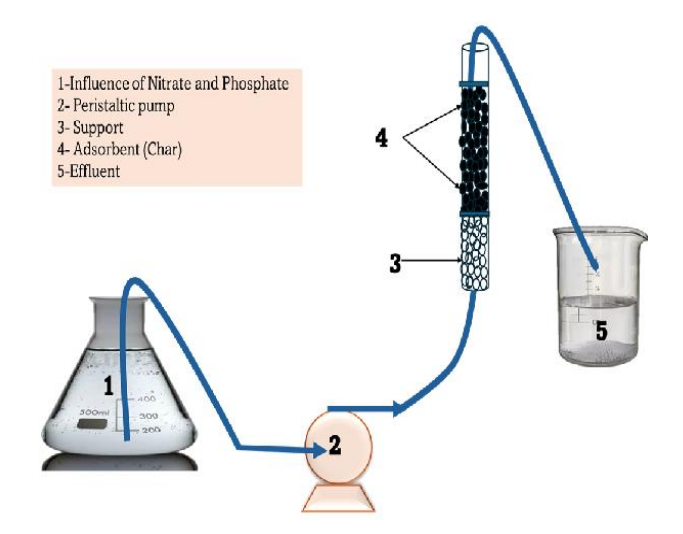


Fig. 2 Schematic diagram of Fixed Bed Column

¹/PO₄ ³ solution collected at various periods from the column exit

2.8 Assessment of column performance

The timing of breakthrough emergence and the configuration of the breakthrough curve are critical attributes for assessing the functionality and responsiveness of fixed-bed column adsorption. Standardly stated as adsorbed concentration, the breakthrough curves reveal phosphate and nitrate loading characteristics that may be extracted from solution with a fixed-bed column. For a specific bed height and time or amount of effluent, the following concentrations can be considered: inlet concentration (C_0), outflow concentration (C_t), or normalized concentration (C_t / C_0). One way to determine the effluent volume (V_{eff}) is by

$$V_{eff} = Qt_{total} (8)$$

where t_{total} and Q are the total flow time (min) and volumetric flow rate (mL/min). To determine the total adsorbed quantity (up to a column capacity), the area beneath the breakthrough (A) curve, typically obtained through the integration of the adsorbed concentration versus time plot, is one useful metric to evaluate. Using a specified input concentration and flow rate, the total adsorbed quantity q_{total} (mg) within a column can be ascertained by:

$$q_{total} = \frac{Q}{1000} \int_0^t (C_o - C_t) dt \tag{9}$$

As a result of solving equations (10), equilibrium uptake, or the optimum capacity of the column q_{eq} (mg/g), represents the amount of adsorbed material per gram of adsorbent (w) following the total flow duration (Ahmad and Hameed, 2010).

$$q_{eq} = \frac{q_{total}}{w} \tag{10}$$

2.9 Dynamic Adsorption Models

2.9.1 The Yoon-Nelson Model

Yoon and Nelson (YOON and and NELSON, 1984) established a model based on the idea that the adsorption possibility and the quantity of adsorbate breakthrough on the adsorbent are connected to the drop in adsorbate molecule adsorption. This is the Yoon-Nelson model, which is a simplified representation of a system with only one part:

$$\ln \frac{c_t}{c_o - c_t} = K_{YN} * t - \tau * K_{YN}$$
 (11)

The rate of velocity constant, K_{YN} (min⁻¹), and the time necessary for 50% adsorbate breakthrough, τ (min), are input into the equation. The values of K_{YN} and τ are obtained from the slope and intercept of the linear graph of ln [Ct/ (Co-Ct)] versus time (t).

2.9.2 Thomas Model

A model proposed by Thomas (Thomas and HENRY THOMAS Vol, no date), Adsorption without internal or exterior diffusion constraints is possible with this material. Here is how Thomas' theory can be expressed in a linear form:

$$\ln\left(\frac{c_o}{c_t} - 1\right) = \frac{\kappa_{TH}q_o w}{Q} - \kappa_{TH}C_o t \tag{12}$$

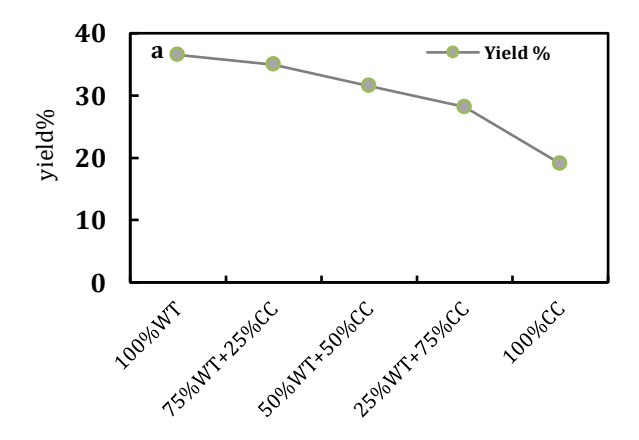
where k_{Th} (ml/min.mg) denotes the coefficient of Thomas rate constant; Q (mL/min) represents the flow rate; q_o (mg/g) indicates the equilibrium uptake of nutrients per gramme of the adsorbent (char); W (g) signifies the mass of the adsorbent; C_o (mg/L) refers to the inlet nutrient concentration since C_t (mg/L) is the outlet concentration at time t; and t total (min) denotes the flow duration.

3. Result and Discussion

3.1 Influence of Waste Tire/Corn Cob Blend Composition

Figure 3 illustrates the yield and utilization of NO₃⁻¹ and PO₄³ from various char samples subjected to continuous processing for 180 minutes at an operating temperature of 600 °C. Figure 3a illustrates that char yield diminishes as corn cob increases from 0% to 100%, reducing production from 35.8% to 19.06%. Due to its composition consisting of carbon black and anti-wrinkle agents, char produced from 100% waste tires exhibits resistance to disintegration, with the fixed carbon (FC) content of waste tire material rubber (45.15%) surpassing that of raw corn cob (1.34%)(Wang *et al.*, 2020). Furthermore, the char production declines as the biomass percentage rises, as the decomposition of organic matter in the biomass leads to elevated quantities of alternative products, such as gas and oil (Li *et al.*, 2021).

Table 1 indicates that waste tire char BWT had a lower carbon content than raw tires. However, the char BCC showed a higher carbon content than raw corn cob. The trend in carbon content indicated that waste tires and corn cobs undergo distinct pyrolysis methods; this can be attributed to the complex solid residues generated during tire production, which consist of



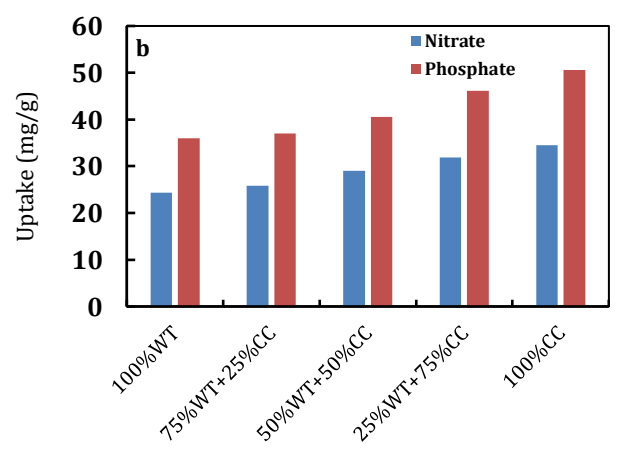


Fig. 3. Effect of blend composition on yield (a) and uptake (b) at (conc. = 700 mg/l, T = 600 $^{\circ}$ C, t = 180 min, and pH = 2)

Table 1Yield, proximate/ultimate analysis, and atomic ratio of chars

Sample	Yield %	Proximate analysis (WT%)			Ultimate analysis (WT% %)				Atomic ratio (wt.%)		
		A	M	V	FC	С	0	N	S	O/C	N/C
Waste tiers	-	4.51	3.24	47.10	45.15	91.81	6.25	1.31	0.63	0.07	0.0143
BWT	35.92	6.68	1.80	44.90	46.63	78.29	16.9	0.53	4.28	0.22	0.0068
75%WT+25%CC	34.98	6.05	1.34	47.27	45.34	81.52	14.84	0.40	3.25	0.18	0.0049
50%WT+50%CC	31.54	4.82	1.04	47.40	46.74	84.75	12.78	0.27	2.22	0.15	0.0031
25%WT+75%CC	28.18	4.56	2.36	47.55	45.53	87.97	10.72	0.13	1.18	0.12	0.0015
BCC	19.06	0.66	2.76	49.79	46.79	91.2	8.66	0.00	0.15	0.09	0.0000
Corn cobs	-	1.60	5.16	75.92	17.32	54.6	45.29	0.00	0.11	0.83	0.0000

*The CNOS content of 75%WT+25%CC,50%WT+50%CC, and 25%WT+75%CC was calculated based on the sample's weight ratio of the waste tire and corn coh.

carbon black (25-35 wt.%), rubber (60-65 wt.%), and various promoters and fillers. Furthermore, pyrolysis produces carbon emissions as small molecules, such as CO, CH₄, CO₂, and others. Agriculture, shown by a corn cob, represents a type of lignocellulosic biomass consisting of macromolecules such as hemicellulose, cellulose, and lignin (Wang *et al.*, 2020). During decomposition, hemicellulose and cellulose degrade rapidly at lower temperatures (230 to 420 °C), but lignin decomposes at higher temperatures (160 to 900 °C) (Yang *et al.*, 2017).

The carbon (C) value in the co-pyrolysis increased, whereas the sulfur (S) content decreased, alongside an elevated biomass level. This was increasingly linked to the higher organic matter concentration in lignocellulosic biomass relative to waste tires (Yin, Liu and Ren, 2019). The oxygen (O) level in char samples diminished as a result of the decline of carbon-bound oxygen groups in organic matter throughout WT and CC pyrolysis (Li *et al.*, 2021).

The polar group content of char can be deduced from its O/C ratio, which typically decreases as the biomass proportion increases, indicating an improvement in char's hydrophobicity to the absence of oxygenated binding(Vijayaraghavan and Balasubramanian, Furthermore, chars exhibit greater resistance to environmental, biological, and chemical degradation owing to their reduced O/C ratio, hence augmenting their stability(Zhang et al., 2020). The proximate analysis of waste tires and biomass (CC) evaluation is essential for assessing the energy-conversion potential of renewable sources. As expected, the waste exhibits a wide range of properties. The ash content of waste tires (4.85%) was higher than the biomass of corn cobs waste (1.60%). Further, the relatively low ash content is an important characteristic of biomass, which exhibits good combustion behavior. Waste tiers and Biomass materials with a moisture content of less than 10% are considered suitable for pyrolysis(Ahmad et al., 2017). Fixed carbon was the combustible material remaining after devolatilization(Raza and Abu-Jdayil,

Figure 4 illustrates the crystalline phases of various chars. Various crystalline phases were identified in BWT and BCC. The crystalline phases of the co-pyrolyzed chars varied according to the percentage of corn cobs added. The XRD pattern of biochar made from biomass like corn cobs

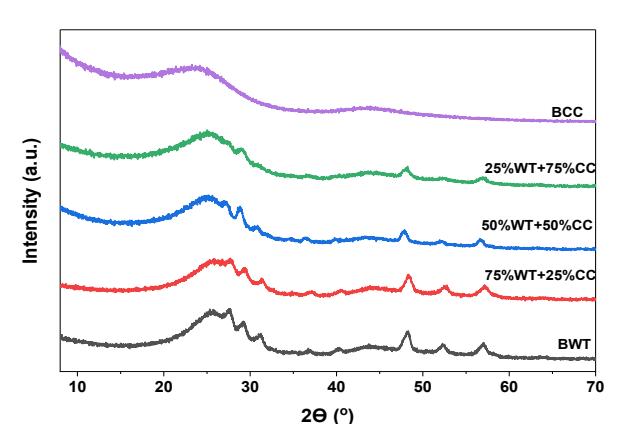


Fig.4. XRD pattern of different chars

shows a mostly amorphous structure. This is because the main organic components of biomass, such as cellulose, hemicellulose, and lignin, break down during pyrolysis. Instead of forming crystalline graphite-like phases, these biopolymers turn into amorphous carbon structures. As a result, the diffraction pattern has broad and weak peaks at $2\theta = 20-30^\circ$, which indicates there is little long-range crystallinity. The amorphous carbon matrix usually contains many surface functional groups and has a very porous structure, which increases its adsorption capacity and surface reactivity. In contrast, biochar made from discarded tires contains more inorganic and metallic materials, leading to stronger diffraction peaks and a higher level of crystallinity.

From Figure 3b, the increases in the biomass (corn cobs) from 25% to 75% exhibited an enhancement of (NO_3^{-1} and PO_4^{-3}) uptakes from (25.87 to 31.85) mg/g for NO_3^{-1} and (37.06 to 46.18) mg/g for PO_4^{-3} , In Table 2, the char surface area obtained from biomass (CC) had a larger specific surface area and a high proportion of micropores of 79.55% than that obtained from waste tires. The specific surface areas of the co-pyrolysis-derived chars were high after adding biomass (CC), and the proportion of micropores increased after the addition of corn cob, especially for the char with a high corn cob ratio. On this basis, the various porous-structured distributions exhibit

Table 2
Porous constructions of various chars

1 010us constructions of va						
Sample	$S_{BET}(m^2/g)$	$S_{micro}(m^2/g)$	$S_{\text{external}}(m^2/g)$	$V_{pore}(cm^3/g)$	D _{pore} (nm)	S_{micro}/S_{BET}
BWT	68.35	0.5090	67.84	0.145	8.522	0.74
75%WT+25%CC	76.09/145.78	25.95/75.57	50.13/70.21	0.101/0.16	5.342/6.96	34.11/51.84
50%WT+50%CC	108.33/223.21	58.11/150.63	50.22/72.58	0.124/0.18	4.583/5.39	53.65/67.48
25%WT+75%CC	185.63/300.64	122.43/225.69	63.21/74.94	0.143/0.196	3.098/3.83	65.95/75.07
BCC	378.06	300.75	77.31	0.214	2.265	79.55

^{*}The data before "/" were obtained from the analysis, and after "/" were calculated following the proportion of waste tiers and corn cobs.

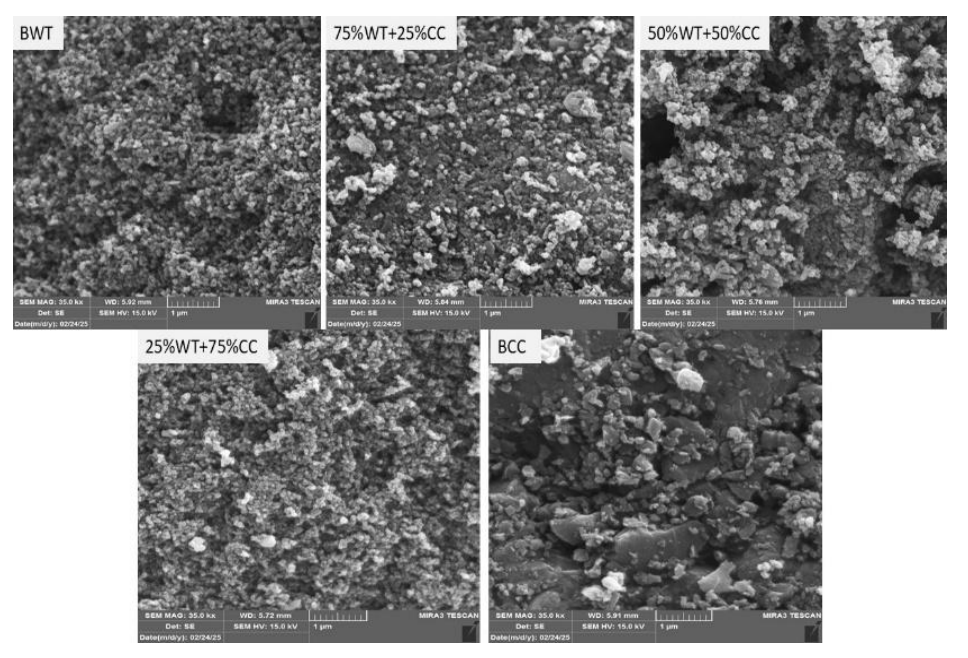


Fig. 5. FE-SEM images of different char

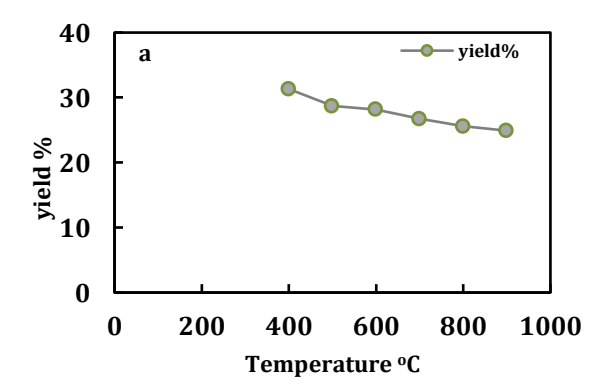
different effects on the adsorption characteristics (Jeguirim et al., 2018).

The theoretical estimates of porosity variables for the three co-pyrolysis chars were computed based on the corresponding real values of BWT and BCC. The predicted BET and micropore surface areas associated with these co-pyrolyzed chars exceeded the actual values, indicating that co-pyrolysis exhibited significant synergetic effects. The theoretical estimate of the external surface area of the co-pyrolyzed char approximated the exact value(Huang *et al.*, 2017). Therefore, the best char was prepared at 25% WT+75%CC

Figure 5 shows the structure of char samples from waste tires (WT), corn cobs (CC), and their mixes (75%WT+25%CC, 50%WT+50%CC, and 25%WT+75%CC). The FE-SEM analysis reveals that the blending ratio of waste tire (WT) and corn cob (CC) affects char morphology. In detail, WT biochar is dense and has low porosity, while CC biochar has a rough, highly porous surface. Blending these materials creates intermediate structures with adjustable surface features. As the corn cob content increases, so do pore formation, surface roughness, and texture, mainly due to volatile release during pyrolysis. Conversely, tire-derived carbon increases the hybrid chars' mechanical stability and carbon density. In short, these results show that mixing different waste materials enables the production of chars with specific features. Therefore, these mixes offer a promising route to convert waste into useful carbon products for environmental and industrial applications.

3.3 Influence of Pyrolysis Temperature

Temperature significantly influences the uptake of (NO_3^{-1}) and PO_4^{-3}) and char production. Figure 6 illustrates the effect of temperature on yield and the uptake of NO_3^{-1} and PO_4^{-3} by the optimal char (25%WT+75%CC). Figure 6a demonstrates that when the temperature increases from 400 to 900 °C, the yield diminishes from 32.06% to 23.94%. As the pyrolysis temperature increases, more volatile components will be lost. Elevated temperatures may induce dehydration of hydroxyl groups and thermal degradation of cellulose and lignin (Gai *et al.*, 2014). At



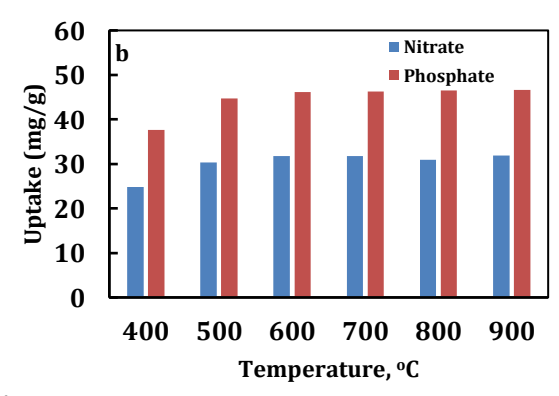
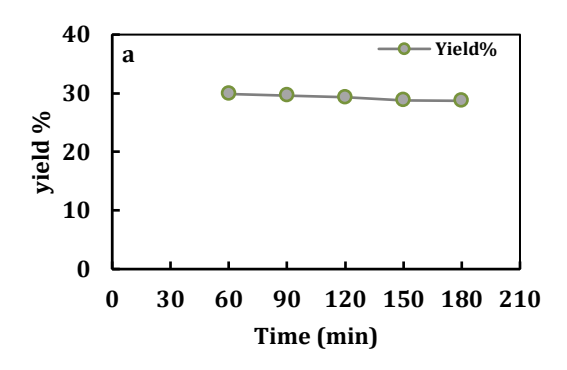


Fig. 6. Effect of temperature on yield (a), and uptake (b) at (conc. = 700 mg/l, T = $600 \,^{\circ}\text{C}$, t = $180 \,\text{min}$, and pH = 2).

temperatures beyond 500° C, a minimal falling rate is observed, indicating the establishment of a stable structure. Figure 6b shows that the (NO₃-¹ and PO₄-³) uptakes increase from (24.87 to 31.28) mg/g and (37.64 to 45.81) mg/g for NO₃-¹ and PO₄-³, respectively. A rise in temperature from (700 to 900) °C at 180 min, the uptake for both (NO₃-¹ and PO₄-³) decreased due to structural changes in the char at high temperatures



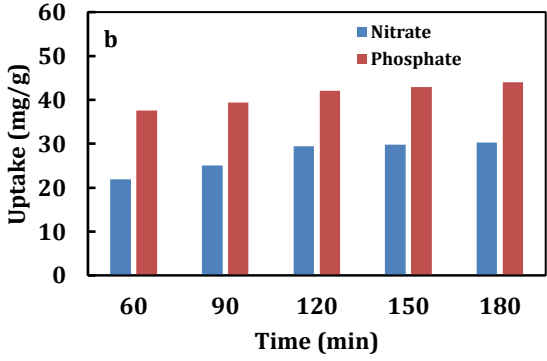


Fig. 7. Effect of time on yield (a), and uptake (b) at (conc. = 700 mg/l, T = $600 \, ^{\circ}\text{C}$, t = $180 \, \text{min}$, and pH = 2).

3.3 Influence of Pyrolysis Time

Figure 7a illustrates the time influence on yield and (NO_3^{-1}) and PO_4^{-3}) uptake of char at the most efficient composite and temperature. The char yield fell steadily from 29.87% to 28.70% with a rise from 60 to 180 min. Figure 7b illustrates that PO_4^{-3} and NO_3^{-1} uptake by char rises from 37.61 to 44.85 mg/g for PO_4^{-3} and 21.93 to 30.28 mg/g for NO_3^{-1} , respectively. Over residence lengths varying from 60 to 120 minutes, there was a large increase in char absorption, whereas no significant difference was detected between samples given for 150 min and 180 min. Assessing all of these and PO_4^{-3} , respectively. A rise in temperature from (700 to 900) °C at 180 min, the uptake for both (NO_3^{-1}) and PO_4^{-3} 0 decreased due to structural changes in the char at high temperatures

3.4 Characterization of Best Char

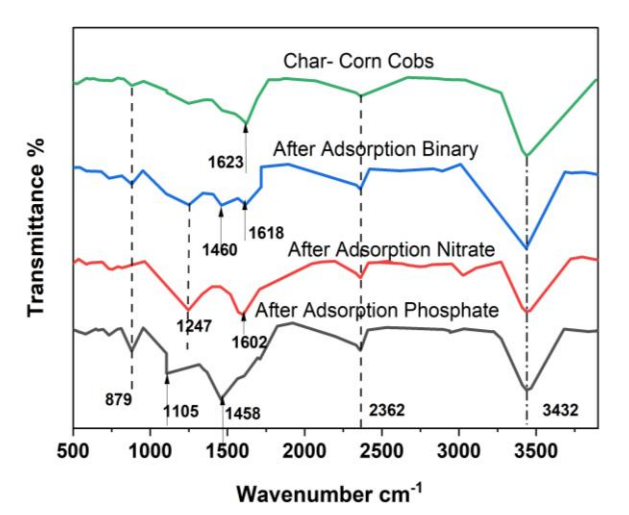
From the preceding results, the best conditions to prepare char are 25% WT+75% CC composite, 500°C temperature, and 120 min time. The yields and the ultimate, proximate parameters gained under these conditions were 29.29%, carbon (C) 88.19 wt.%, oxygen (O) 10.74 wt.%, and sulfur (S) 1.07 wt.% content in the blended waste. In Figure 8a, the capacity of adsorption char is markedly influenced by its surface groups. Infrared spectroscopy using the Fourier transformation is essential for examining the surface characteristics before and after the pollutants' adsorption. Several active groups, like the (OH) stretch vibration in the range 3432 cm⁻¹. This peak showed the presence of adsorbed moisture in the material, indicating that the waste was hydrophilic(Raza and Abu-Jdayil, 2023).

The peaks at 1623 cm⁻¹ showed the stretching of carbonyl (C=O) groups, and the peak at 1105 cm⁻¹ represented the stretching of C-O. Generally, proton donors can be carboxyl or hydroxyl groups. Adsorbates can form coordination complexes with deprotonated carboxyl and hydroxyl groups.

In Figure 8a, the adsorption capacity of char is markedly influenced by its surface groups. Infrared spectroscopy using the Fourier transform is essential for examining the surface characteristics before and after the pollutants' adsorption. Several active groups, like the (OH) stretch vibration in the range 3432 cm⁻¹. This peak showed the presence of adsorbed moisture in the material, indicating that the waste was hydrophilic(Raza and Abu-Jdayil, 2023). The peaks at 1623 cm⁻¹ showed the stretching of carbonyl (C=O) groups, and the peak at 1105 cm⁻¹ represented the stretching of C-O. Generally, proton donors can be carboxyl or hydroxyl groups. Adsorbates can form coordination complexes with deprotonated carboxyl and hydroxyl groups. The carbonate content of the different forms of biochar is indicated by the peak at 879 cm⁻¹ (Eduah *et al.*, 2019).

In phosphate adsorption on char-corn cobs, the intensity and shape of the O-H stretching at 3432 cm⁻¹ broad peak is due to the interaction between the phosphate ions and hydroxyl groups on the char surface. The current peak at 2362 cm⁻¹ asymmetric stretching of C=O is adsorbed on the surface or related to P-H or P-O-H bonds from phosphate species; its presence is due to chemical interaction or complex formation with phosphate ions.

The peak at 1458 cm⁻¹ was related to P-O symmetric stretching. The 879 cm⁻¹ low-frequency peaks could correspond



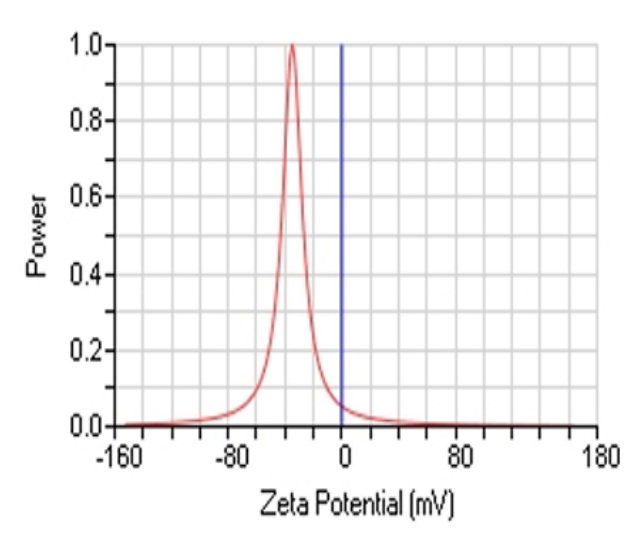


Fig. 8. FTIR before and after adsorption of nutrients (a) and zeta potential of 25% WT+75% CC(b).

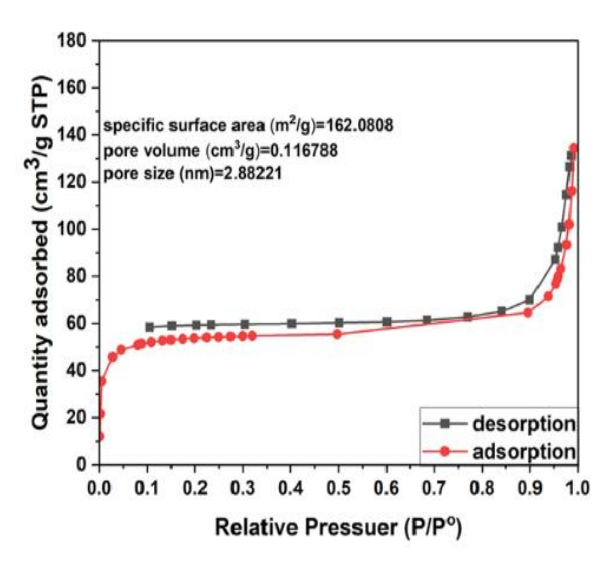
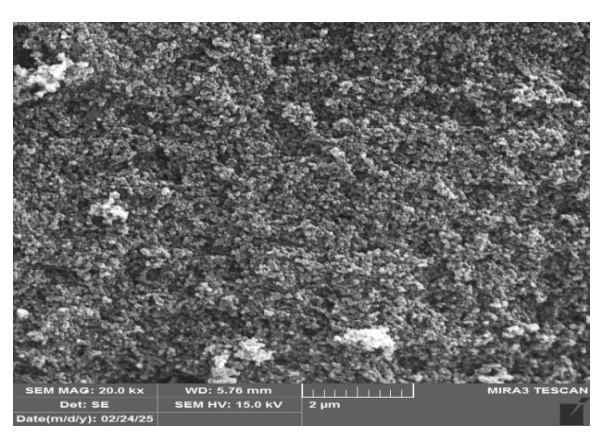


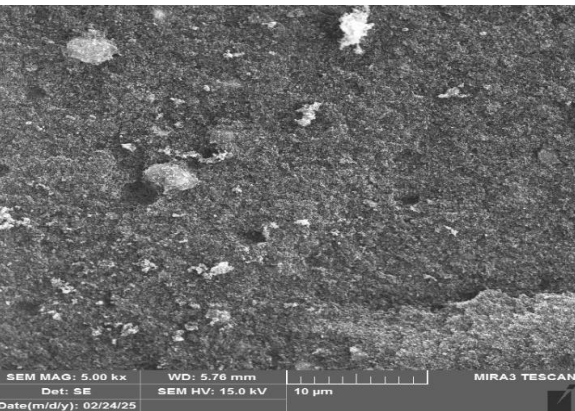
Fig. 9. N_2 adsorption-desorption isotherm of composite (25%WT+75%CC).

to the bending vibration of P-O bonds. In nitrate adsorption on char-corn cobs, the change in intensity of the hydroxyl groups (-OH) indicates that hydrogen bonding or electrostatic interactions occur with nitrate ions. The peak at 2362 cm⁻¹ appears to reflect structure or surface change by nitrate adsorption. The 1602 cm⁻¹ shift from the original char peak is due to the nitrate and carbonyl group (C=O) interaction(Aswin Kumar et al., 2021; Varela, Moreno-Aldana and Agámez-Pertuz, 2024). Following the adsorption of the PO₄-3/NO₃-1 (binary) mixture, the FTIR analysis revealed a reduced peak intensity, which may be ascribed to the interaction of phosphate and nitrate through hydrogen bonds aided by the surface functional groups of the char. Additionally, spectral alterations were observed, including the change in position or disappearance of peaks associated with carboxyl and hydroxyl groups, with the peak at 2358 cm⁻¹ disappearing because of the interaction of PO₄-3 / NO₃-1. The peak at 1618 cm⁻¹, a slight shift from the original, indicates interaction between (PO₄-3/NO₃-1) and carbonyl or aromatic groups on the char surface (Cheng et al., 2021). A peak at 1460 cm⁻¹ indicates that both phosphate and nitrate ions are present on the surface of the char. The shifts in the spectra demonstrate that the aromatic ring structures, carboxyl groups, and hydroxyl groups on the char surface are responsible for nitrate and phosphate binding.

Simultaneously, the Zeta potential affects the adsorption capability by influencing electrostatic interactions and the charge of the surface. The zeta potential was evaluated for the charge of the adsorbent surface by incorporating 0.2 g of the char into 50 ml of purified water, resulting in an initial suspension with a pH of 7.5 ± 0.5 . The potential for char zeta varies with the solution pH level. Char has a negative zeta potential in neutral to slightly acidic environments (-10 mV to -40 mV), and a positive one in basic ones. Figure. 8b shows that the char surface has a negatively charged zeta potential of -34.74 mV(Yang $et\ al.$, 2017; Cheng $et\ al.$, 2021).

An essential metric for assessing an adsorbent's porous structure is its specific surface area. Figure 9 displays the 25% WT+75 % CC composite's specific surface area and the N_2 adsorption isotherm. Products with a large surface area for adsorption on a monolayer and a porous structure for condensation through capillaries fall under type IV of the adsorption isotherm. Similar to open-ended cylindrical pores, Type H3 hysteresis is observed in the pore system for the adsorption-desorption curve. When determined with the BET





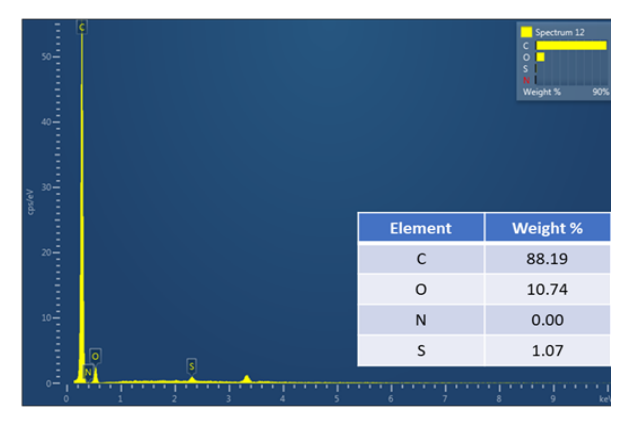


Fig. 10. FESEM and EDX image of composite char (25%WT+75%CC).

technique, the 25% WT+75 % CC material had a much higher specific surface area (162.0809 m²/g) than other char materials. The significant adsorption possibility of both nitrate and phosphate was believed to be due in large part to this very particular surface area (Luo *et al.*, 2015). Figure 10 illustrates a char porous materials field emission scanning electron micrograph (FESEM) with surface-attached particles of varying shapes.

3.5 Adsorption Isotherm

The adsorption isotherm investigations of NO_3^{-1} and PO_4^{-3} on (25% WT + 75% CC) are shown in Figure 11. In Table 3, the results of fitting three different adsorption isotherm models, including the parameters and correlation coefficients (R²), are shown. For nitrate, the q_m equals 37.44 mg/g, while for phosphate, the value is 62.15 mg/g. The highest R² values best fit the Sips isotherm, compared with the Langmuir and the Freundlich models. Given this heterogeneity in the distribution

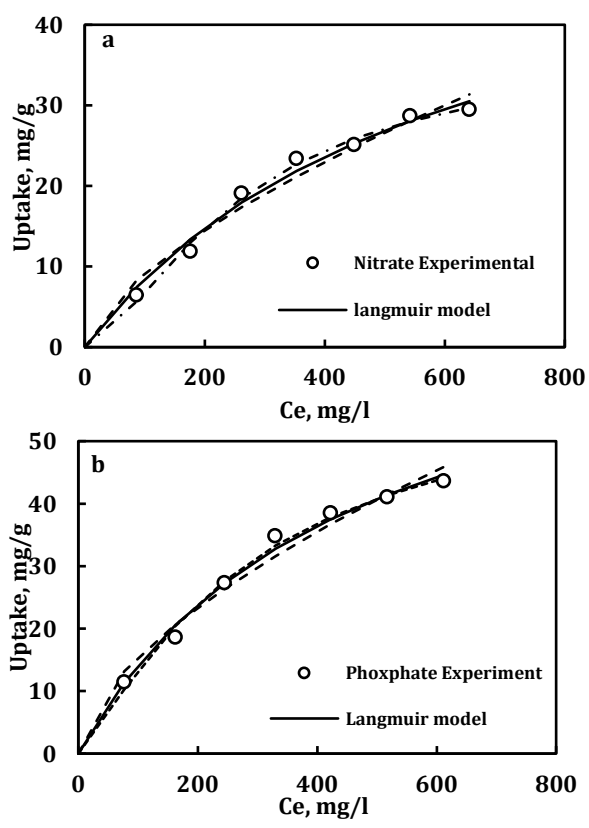


Fig. 11. Adsorption isotherm on char for nitrate(a) and phosphate (b)

Table 3 Parameters of (NO₃⁻¹ and PO₄⁻³) adsorption isotherms.

	- F		
Model		Nitrate	Phosphate
Langmuir	q_{m}	59.19	77.23
	K_1	0.0017	0.0022
	\mathbb{R}^2	0.9899	0.9940
Freundlich	K_{f}	0.4367	0.9599
	n	1.51	1.66
	\mathbb{R}^2	0.9781	0.9846
Langmuir- Freundlich	q_s	37.44	62.15
model	K	0.0002	0.001
	m	0.65	0.82
	\mathbb{R}^2	0.9957	0.9953

of active sites, nutrient adsorption by char is of the multilayer kind(Yin, Liu and Ren, 2019). Therefore, the sips model shows that the adsorption of PO_4^{-3} and NO_3^{-1} onto char is a physicochemical adsorption process that not only exists on the

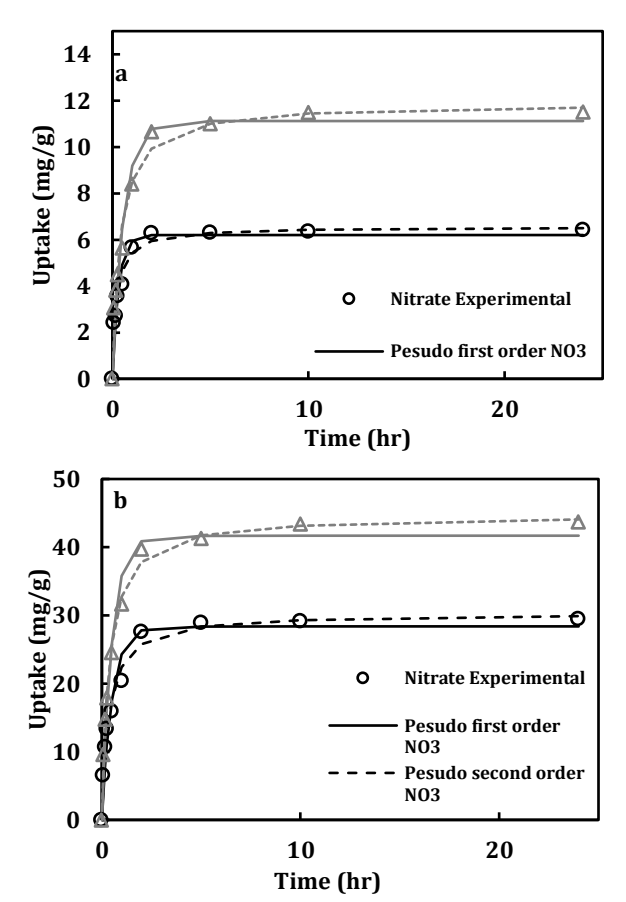


Fig. 12. Adsorption kinetics on char for nitrate and phosphate at (a) 100 mg/g and (b) 700 mg/g.

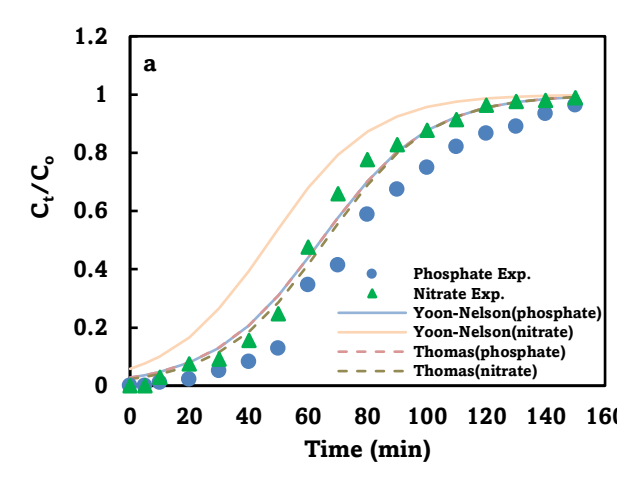
outer surface of the biochar but also exists in the micropores of the biochar (Cheng *et al.*, 2021).

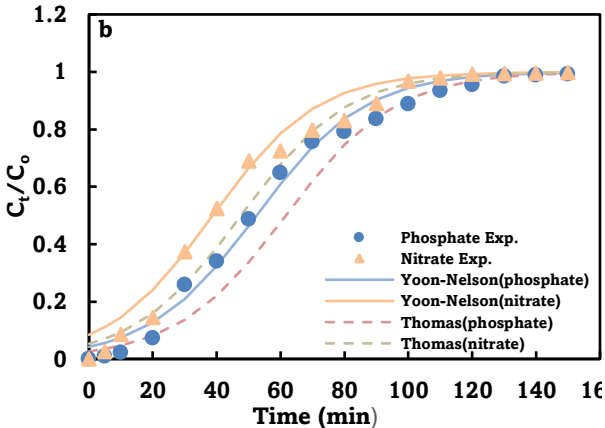
3.6 Adsorption Kinetics

Figure 12 displays the results of fitting the experimental kinetics data for NO₃-¹ and PO₄-³ adsorption on co-pyrolysis char, which were obtained from Eq. (2), with (pseudo-first order and pseudo-second order) (Eqs. (6) and (7)). Table 4 displays the derived constants and R² values from kinetic model equations at different inlet adsorbate concentrations. In contrast to the low R² magnitudes for NO₃-¹ and PO₄-³ obtained by the pseudo-first-order equation shown in Table 4, the pseudo-second-order equation yields high R² values (Table 4). The pseudo-second-order kinetic model adequately described the adsorption kinetics, and the calculated qe values for NO₃-¹ and PO₄-³ agree well with the experimental qe values. Moreover, this table illustrates a significant discrepancy between the experimental and estimated adsorption capacities, indicating an inadequate

Table 4Characteristics of different kinetic models for the adsorption of NO₃⁻¹ and PO₄⁻³ onto a mixture of 25% WT and 75% CC char.

Mode	el	Niti	rate	Phosphate		
	-	100 mg/L	700 mg/L	100 mg/L	700 mg/L	
Pseudo-first order	q _e (mg/L)	6.20	28.38	11.12	41.69	
	K ₁ (hr ⁻¹)	3.16	1.94	1.75	1.95	
	R^2	0.9615	0.9681	0.9739	0.9811	
Pseudo-second	q _e (mg/L)	6.56	30.33	11.89	44.47	
order	$K_2(g/mg hr)$	0.74	0.09	0.21	0.06	
	R^2	0.9798	0.9871	0.9830	0.9957	





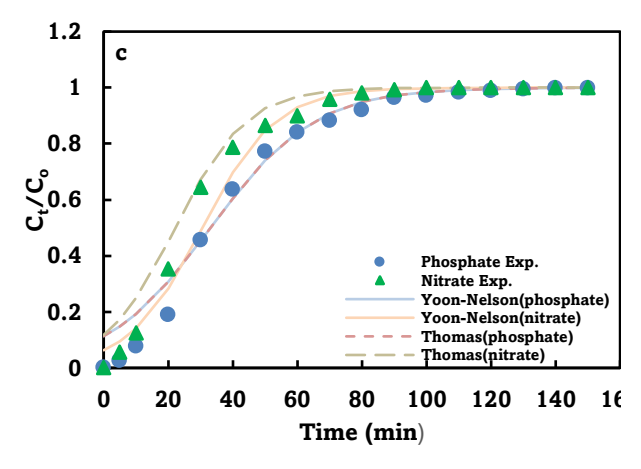


Fig.13. Experimental breakthrough curves at different initial concentrations of binary solution on char (a=100 mg/L, b=300 mg/L, and c=600 mg/L, flow rate 10ml/min, H=10 cm, pH=2)

fit of the pseudo-first-order model to the experimental data. In other words, the adsorption of NO₃-1 and PO₄-3 on char is controlled by the pseudo-second order kinetic model posits that the rate-limiting phase involves the interaction between two substance particles and is commonly employed to characterize chemical adsorption(Divband Hafshejani *et al.*, 2016). Several authors have successfully represented experimental kinetic data of nutrient adsorption by char using the pseudo-second-order model(Yin, Liu and Ren, 2019; Adauto and Sun-Kou, 2021).

3.7 Effect of Initial Concentration

The influence of different initial solute concentrations was examined using concentrations of 100, 300, and 600 ppm, a bed height of 10 cm, and a flow rate of 10 ml/min. Figure 13 illustrates that the bed reaches saturation rapidly at elevated concentrations of PO₄-3/NO₃-1, resulting in an earlier breakthrough time. This can be elucidated by the inverse relationship between initial concentration and adsorption equilibrium time; lower initial solute concentrations necessitate prolonged contact time to achieve adsorption equilibrium. The adsorption rate was constrained by diffusion; thus, factors affecting diffusion substantially impact the adsorption rate. The elevated inflow concentration resulted in effectively occupied adsorption sites, producing a more pronounced breakthrough curve and expedited saturation of the bed (Baboli and Bafkar, 2023; Wang, Amano and Machida, 2024). Table 5 displays all of the adsorption capacities and the determined depletion times.

3.8 Effects of Flow Rate

Figure 14 illustrates the experimental results, including breakthrough curves for NO₃-1 /PO₄-3 at varying flow rates (5, 10, and 15 ml/min) with an intake concentration of 300 ppm and a bed height of char 10 cm. Analysis of the statistics indicates that at a volumetric flow rate of 15 ml/min, there is an initial guick removal of anions, followed by a decrease in the removal rate, ultimately leading to saturation. This may indicate an elevation in flow rate, resulting in reduced breakthrough and fatigue durations and an extended mass transfer zone. As the volumetric flow rate rises, the contact duration between the adsorbate and adsorbent reduces, resulting in limited time for lateral diffusion through the char bed and insufficient liquid distribution throughout the fixed bed. This ultimately results in reduced diffusivity of the solute between the particles of adsorbent and the film liquid surrounding them, causing a decline in the boundary layer and an increase in resistance to mass transfer related to the adsorption process within the bed (Abdipour et al., 2024).

3.9 Effect of Bed Height

The bed height is the primary variable in a column of fixed-bed adsorption. The bed's height is crucial when designing a bed with a fixed adsorption column. Breakthrough curves for 5, 10, and 15 cm char beds at 300 ppm initial concentration and 10 ml/min flow rate are shown in Figure 15. It is clear that as the bed length grows, the substance's resistance time and time to breakthrough in the column both rise, enabling molecules to enter the adsorbent particles. On the other hand, the bed becomes saturated more quickly at lower bed heights compared to higher ones. The adsorbent's adsorption area grows in tandem with the length of the bed and the overall number of binding sites(Olgun, Atar, and Wang, 2013; Baboli and Bafkar, 2023).

3.10 Column Study

3.10.1 Prediction Utilizing the Yoon-Nelson model

The Yoon-Nelson model was used to study the breakthrough behavior at the 50% breakpoint for phosphate and nitrate under different initial concentrations, flow rates, and bed heights. The constants K_{YN} and τ were calculated by plotting ln (ct/(co-ct)) vs τ , using the slope and intercept. Table 6 shows the calculated values for K_{YN} and τ .

Table 6 illustrates that the constant flow rate of K_{YN} grows while the time τ diminishes with rising initial concentration and

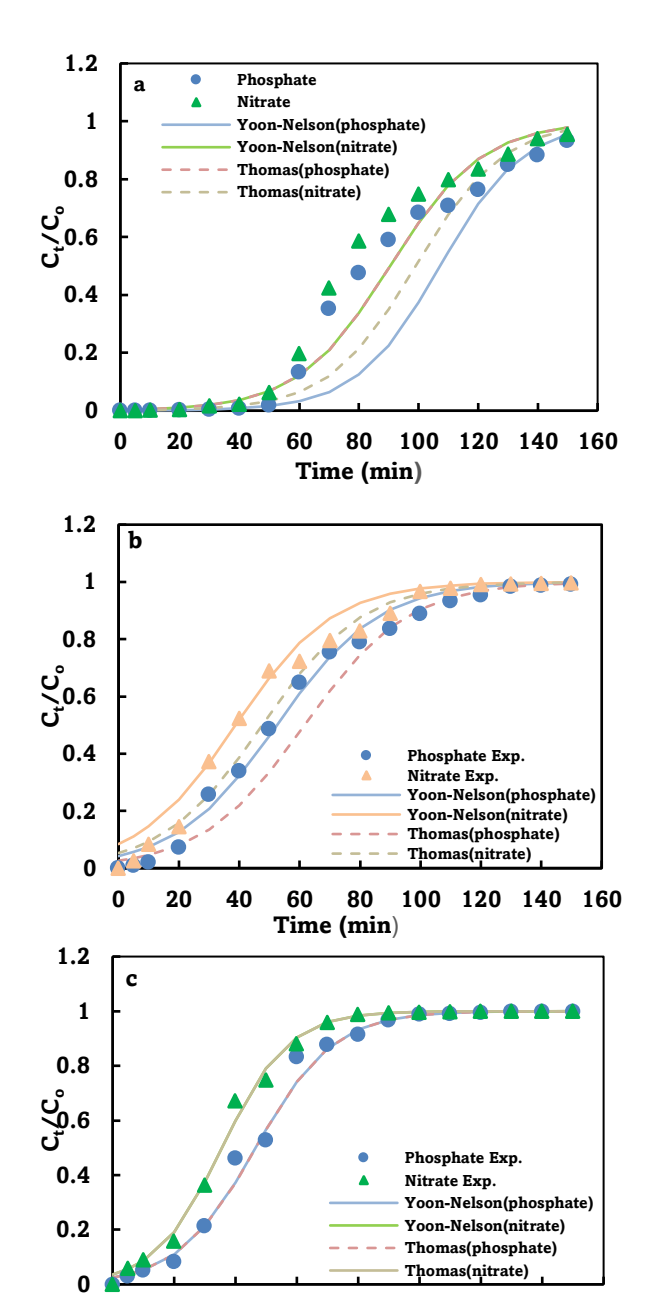


Fig.14. Experimental breakthrough curves at different flow rates of binary solution on char (a= 5ml/L, b=10ml/L, and c= 15ml/L, conc 300 mg/L, H=10 cm, pH=2).

Time (min)

60

80

100 120 140 160

0

20

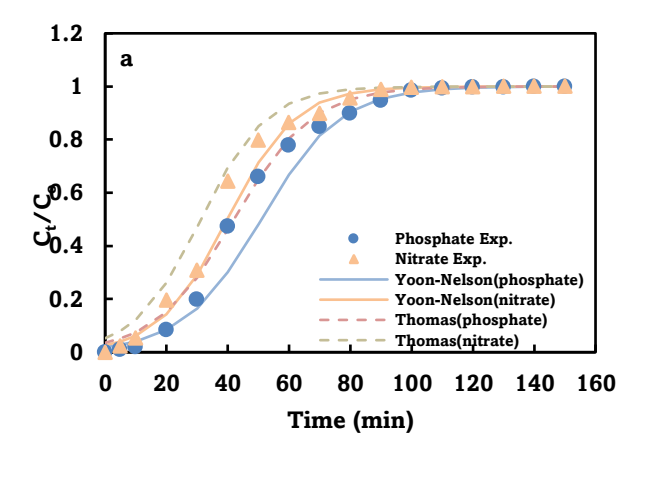
40

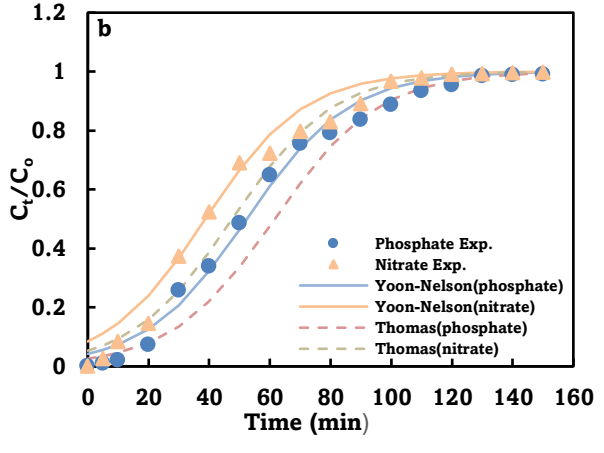
flow rate. An elevated initial concentration generates a heightened driving force for the transfer of mass, leading to a more rapid saturation of adsorbent sites and expedited adsorption (Abdipour *et al.*, 2024). With a rise in flow rate, the adsorbate arrives in the column. The height of the bed rose as the time value τ increased. The K_{YN} decreased due to the increased availability of adsorbent. The process became more controlled with expanded total surface area and prolonged contact time. As a result, the process became more efficient, increasing the likelihood of adsorbate molecules being collected before breakthrough (Darweesh and Ahmed, 2017)

3.10.2 Prediction Utilizing the Thomas model

The Thomas model was applied to column sorption data. This determined the effect of changing initial concentrations of PO_4^{-3}/NO_3^{-1} (50-300 mg/L), flow rates (5–15 ml/min), and bed height (5-15 cm).

A linear plot of $\ln \left[(c_o/c_t) - 1 \right]$ vs. t was used. From the slope and intercept, the adsorption rate constant (K_{th}) and maximum adsorption capacity (q_o) were determined according to Eq. (12). Moreover, the calculated values of K_{th} and q_o , along with the R^2 , are presented in Table 7. These relatively high R^2 values under all operating conditions suggest that the model is suitable for describing the column sorption data. When the initial concentration increased from 50 mg/L to 300 mg/L, the constant rate (K_{th}) decreased, while the adsorbed solid phase (q_o) increased from 5.28 mg/g to 16.28 mg/g for phosphate and





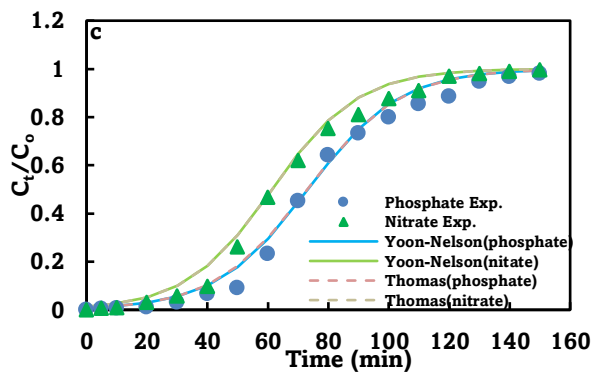


Fig.15. Experimental breakthrough curves at different bed heights of binary solution on char (a=5 cm, b=10cm, and c=15cm, conc. 300 mg/L, flow rate=10 ml/min, pH=2)

Table 5

Various inflow concentrations, flow rates, and bed heights were used to measure the column data parameters.

Inlet	et Bed heights Flow		q_{total}	(mg)	q _{eq} (n	q _{eq} (mg/g)	
concentration	(cm)	(ml/min)	PO_4^{-3}	NO_3^{-1}	PO_4^{-3}	NO_3^{-1}	
(mg/L)							
50	10	10	75.84	69.38	12.44	11.38	
150	10	10	194.74	180.14	31.94	29.54	
300	10	10	339.86	312.18	55.74	51.20	
150	5	10	181.76	169.50	59.58	55.56	
150	15	10	227.30	212.10	25.97	24.24	
150	10	5	120.47	116.06	19.76	19.04	
150	10	15	217.92	250.67	44.60	41.11	

Table 6

Yoon-Nelson parameters in various circumstances using linear regression analysis

Inlet	Bed	Flow rates	K _{YN} (1	K _{YN} (1/min)		τ (min)		22
concentration	heights	(ml/min)	PO_4^{-3}	NO_3^{-1}	PO_4 -3	NO_3^{-1}	PO_4^{-3}	NO_3^{-1}
(mg/L)	(cm)							
50	10	10	0.0551	0.0589	64.44	47.33	0.9859	0.9642
150	10	10	0.0595	0.0615	52.45	38.76	0.9912	0.9895
300	10	10	0.0621	0.0883	33.09	30.55	0.9924	0.9803
150	5	10	0.0775	0.0904	50.92	39.86	0.9767	0.9880
150	15	10	0.0659	0.0701	61.37	89.83	0.9946	0.9963
150	10	5	0.0717	0.0646	107.23	90.52	0.8553	0.9463
150	10	15	0.0789	0.0923	46.65	35.66	0.9915	0.9858

Table 7

Thomas' model parameters are used in different conditions using linear regression analysis

111	omas model para	incluib are at	oca iii aiiiciciii c	Onditions asin	ng micai regre	bbioir ariary bic	,		
	Inlet	Bed	Flow rates	K_{Th} (mL)	K _{Th} (mL/min.mg)		q₀ (mg/g)		\mathcal{E}^2
	concentration	heights	(ml/min)	PO ₄ -3	NO_3^{-1}	PO ₄ -3	NO_3^{-1}	PO ₄ -3	NO_3^{-1}
	(mg/L)	(cm)							
	50	10	10	1.102	1.14	5.28	5.41	0.9857	0.9910
	150	10	10	0.3913	0.4033	15.16	11.72	0.9658	0.9598
	300	10	10	0.207	0.3033	16.28	10.89	0.9924	0.9966
	150	5	10	0.5247	0.6187	20.63	15.33	0.9965	0.9915
	150	15	10	0.436	0.4673	12.52	10.52	0.9945	0.9963
	150	10	5	0.4301	0.456	11.13	12.19	0.9674	0.8848
	150	10	15	0.526	0.6153	17.22	13.16	0.9915	0.9858

from 5.41 m g/g to 10.89 mg/g for nitrate. These results indicate that an increase in the influent concentration modifies the adsorption rate and increases the bed adsorption capacity. Notably, similar results were reported by (Kizito *et al.*, 2016).

A similar pattern was observed as the flow rates increased from 5 ml/min to 15 ml/min. In this case, adsorption rates $K_{\rm th}$ and $q_{\rm o}$ rose in all char beds. This increase can be ascribed to improved mass transfer and a stronger driving force for adsorption. Moreover, accelerated external film diffusion and improved solute molecular access to active sites result from high flow rates, which raise the concentration gradient between the liquid and the adsorbent surface. Furthermore, K_{th} and $q_{\rm o}$ both decreased as the bed height was raised from 5 to 15 cm due to mass transfer resistance (Meng $\it et\,al., 2013$). The drop in $q_{\rm o}$ is likely caused by the adsorbent not being used enough throughout the bed.

4. Conclusion

Co-pyrolysis of waste tires/corn cobs blend with a composition of 25% WT +75% CC exhibited a char with a good remediation

performance against NO₃⁻¹ and PO₄⁻³ from water. The (BET) surface area, average pore size, and total pore volume of the obtained char were 162.0808 m²/g, 2.88221 nm, and 0.116788cm³/g, respectively. The Sips equation showed the best analysis for isothermal data with maximum adsorption capacities of 77.23 and 59.19 mg/g for PO₄-3 and NO₃-1, respectively. The adsorption capacity is high for PO₄-3 and NO₃-¹ in an acidic medium. According to isotherm and kinetic investigations, the multi-layer chemisorption process identified the adsorption of PO₄-3 and NO₃-1 by the char that was made from waste tires and corn cob. The fixed-bed adsorption system performed better with lower binary PO₄-3 / NO₃-1 inlet concentration, diminished feed flow rate, and increased char bed height. The impact of different operating conditions on the breakthrough curve and column performance allowed us to analyze the column's behavior and uptake. The constant parameters for each breakthrough model, including Yoon-Nelson and Thomas, were established as part of the fitting process, the τ for phosphate (33.09-107.23 min) and for nitrate (30.55-90.52 min) and the q₀ for phosphate (5.28- 20.63 mg/g) and for nitrate (5.41-15.33 mg/g), respectively. The models'

speed constants rose as the flow rate increased, indicating that the adsorption kinetics are dictated by external mass transfer.

Author Contributions: Sally A. Hussein: Data curation, investigation, writing—original draft, writing-review, and editing. Muthanna J. Ahmed: Supervision, Writing-Review, and Editing.

Conflicts of Interest: The corresponding author states that there is no conflict of interest.

References

- Abd, M.F. and Al-Yaqoobi, A.M. (2023) 'The feasibility of utilizing microwave-assisted pyrolysis for Albizia branches biomass conversion into biofuel productions', *International Journal of Renewable Energy Development*, 12(6), 1061–1069. https://doi.org/10.14710/ijred.2023.56907.
- Abd, M.F., Al-yaqoobi, A.M. and Abdul-Majeed, W.S. (2024) 'Catalytic Microwave Pyrolysis of Albizia Branches Using Iraqi Bentonite Clays', *Iraqi Journal of Chemical and Petroleum Engineering*, 25(2), 175–186. https://doi.org/10.31699/ijcpe.2024.2.16.
- Abdipour, H., Ghorban Asgarib, Abdolmotaleb Seid-Mohammadib, Alireza Rahmanid, and Reza Shokoohi (2024). 'Investigating the efficiency of fixed bed column containing Fe3O4-ZIF8@eggshell membrane matrix in concurrent adsorption of arsenic and nitrate from water', *Ecotoxicology and Environmental Safety*, 288. https://doi.org/10.1016/j.ecoenv.2024.117359.
- Abdul Wahab, A.I., Soaded Alsaqqar, A., and Kareem Ali, S. (2011). Removal of Phosphorus from Wastewater by Adsorption onto Natural Iraqi Materials, Journal of Engineering. *Journal of Engineering*, 17. https://doi.org/10.31026/j.eng.2011.02.15.
- Adauto, A. and Sun-Kou, M.R. (2021) 'Comparative study of anion removal using adsorbents prepared from a homoionic clay', *Environmental Nanotechnology, Monitoring and Management*, 15. https://doi.org/10.1016/j.enmm.2021.100476.
- Ahmad, A.A. and Hameed, B.H. (2010) 'Fixed-bed adsorption of reactive azo dye onto granular activated carbon prepared from waste', *Journal of Hazardous Materials*, 175(1–3), 298–303. https://doi.org/10.1016/j.jhazmat.2009.10.003.
- Ahmad, M.S., Mehmood, Omar S. Al Ayed, Guangbin Ye, Huibo Luo, Muhammad Ibrahim, Umer Rashid, Imededdine Arbi Nehdi, and Ghulam Qadir (2017) 'Kinetic analyses and pyrolytic behavior of Para grass (Urochloa mutica) for its bioenergy potential', Bioresource Technology, 224, 708–713. https://doi.org/10.1016/j.biortech.2016.10.090.
- Ahmed, M.J. and Dhedan, S.K. (2012) 'Equilibrium isotherms and kinetics modeling of methylene blue adsorption on agricultural wastes-based activated carbons', *Fluid Phase Equilibria*, 317, 9–14. https://doi.org/10.1016/j.fluid.2011.12.026.
- Ahmed, M.J., Hameed, B.H. and Khan, M.A. (2023) 'Recent advances on activated carbon-based materials for nitrate adsorption: A review', Journal of Analytical and Applied Pyrolysis. https://doi.org/10.1016/j.jaap.2022.105856.
- Alsewaileh, A.S., Usman, A.R. and Al-Wabel, M.I. (2019) 'Effects of pyrolysis temperature on nitrate-nitrogen (NO3--N) and bromate (BrO3-) adsorption onto date palm biochar', *Journal of Environmental Management*, 237, 289–296. https://doi.org/10.1016/j.jenvman.2019.02.045.
- Aswin Kumar, Antonysamy Jeyaseelan, Natrayasamy Viswanathan, Mu. Naushad, and Artur J.M. Valente (2021) Fabrication of lanthanum-linked trimesic acid as porous metal organic frameworks for effective nitrate and phosphate adsorption, Journal of Solid State Chemistry, 302. https://doi.org/10.1016/j.jssc.2021.122446.
- Awual, M.R., Akinori Jyo, Toshihiro Ihara, Noriaki Seko, Masao Tamada, and Kwon Taek Lim (2011) 'Enhanced trace phosphate removal from water by zirconium(IV) loaded fibrous adsorbent', Water Research, 45(15), 4592–4600. https://doi.org/10.1016/j.watres.2011.06.009.

- Baboli, N. and Bafkar, A. (2023) 'Nitrate removal from aqueous solutions using nanostructured adsorbents in continuous and discontinuous systems', *Desalination and Water Treatment*, 284, 116–133. Available at: https://doi.org/10.5004/dwt.2023.29164.
- Betancur, M., Arenas, N.C., Martinez, D.J., Navarro, V.M., and Murillo, R. 2020) 'CO2 gasification of char derived from waste tire pyrolysis: Kinetic models comparison', *Fuel*, 273. https://doi.org/10.1016/j.fuel.2020.117745.
- Boeykens, S.P., Piol, M.N., Legal, L.S., Saralegui, A.B., and Vazquez, C.(2017) 'Eutrophication decrease: Phosphate adsorption processes in presence of nitrates', *Journal of Environmental Management*, 203, 888–895. https://doi.org/10.1016/j.jenvman.2017.05.026.
- Braun, J.C.A., Borba, C.E., Godinho, M., Perondi, D., Schontag, J.M., and Wenzel, B.M. (2019) 'Phosphorus adsorption in Fe-loaded activated carbon: Two-site monolayer equilibrium model and phenomenological kinetic description', *Chemical Engineering Journal*, 361, 751–763. https://doi.org/10.1016/j.cej.2018.12.073.
- Cheng, N., Wang, B., Feng, Q., Zhang, X., and Chen, M. (2021) 'Coadsorption performance and mechanism of nitrogen and phosphorus onto eupatorium adenophorum biochar in water', *Bioresource Technology*, 340. https://doi.org/10.1016/j.biortech.2021.125696.
- Darweesh, T.M. and Ahmed, M.J. (2017) 'Adsorption of ciprofloxacin and norfloxacin from aqueous solution onto granular activated carbon in fixed bed column', *Ecotoxicology and Environmental Safety*, 138, 139–145. https://doi.org/10.1016/j.ecoenv.2016.12.032.
- De-Bashan, L.E., Moreno, M., Hernandez, J., and Bashan, Y. (2002)
 Removal of ammonium and phosphorus ions from synthetic wastewater by the microalgae Chlorella vulgaris coimmobilized in alginate beads with the microalgae growth-promoting bacterium Azospirillum brasilense, *Water Research*. https://doi.org/10.1016/S0043-1354(01)00522-X.
- Divband Hafshejani, L. Hooshmand, A., Naseri, A.A., Mohammadi, S.M., Abbasi, F., and Bhatnagar, A.(2016) 'Removal of nitrate from aqueous solution by modified sugarcane bagasse biochar', *Ecological Engineering*, 95, 101–111. https://doi.org/10.1016/j.ecoleng.2016.06.035.
- Eduah, J.O., Nartey, E.K., Abekoe, M.K., Breuning-Madsen, H., and Andersen, M.N. (2019) 'Phosphorus retention and availability in three contrasting soils amended with rice husk and corn cob biochar at varying pyrolysis temperatures', *Geoderma*, 341, 10–17. https://doi.org/10.1016/j.geoderma.2019.01.016.
- Eisenbach, T., Jahromi, B.F., Angenent, V., Pflieger, C., Muhler, M., Schmid, R., Wedler, C., and Span, R. (2025) 'Linking experimental H2O vapor adsorption on biomass char with physicochemical char properties and MD simulation', *Fluid Phase Equilibria*, 597, 114460. https://doi.org/10.1016/j.fluid.2025.114460.
- Fatima, I., Ahmed, M., Vithanage, M., and Iqbal, S. (2021) 'Abstraction of nitrates and phosphates from water by sawdust- and rice husk-derived biochars: Their potential as N- and P-loaded fertilizer for plant productivity in nutrient deficient soil', *Journal of Analytical and Applied Pyrolysis*, 155. https://doi.org/10.1016/j.jaap.2021.105073.
- Gai, X., Wang, H., Liu, J., Zhai, L., Liu, S., Ren, T., and Liu, H.(2014) 'Effects of feedstock and pyrolysis temperature on biochar adsorption of ammonium and nitrate', *PLoS ONE*, 9(12). https://doi.org/10.1371/journal.pone.0113888.
- Ghalandari, V., Hashemipour, H. and Bagheri, H. (2020) 'Experimental and modeling investigation of adsorption equilibrium of CH4, CO2, and N2 on activated carbon and prediction of multicomponent adsorption equilibrium', *Fluid Phase Equilibria*, 508, 112433. https://doi.org/10.1016/j.fluid.2019.112433.
- Han, L., Liu, R., Wang, H., Hu, B., Qiu, M., and Zhang, H. (2022) 'Efficient adsorption of nitrate and phosphate from wastewater by the costeffective Mg/Ca bimetallic oxide composites functionalized peanut shell', *Desalination and Water Treatment*, 261, 159–169. https://doi.org/10.5004/dwt.2022.28503.
- Hasan, H.A., Mohd Saharuddin, S.N.D. and Muhamad, M.H. (2025) 'Unlocking the potential of polyvinyl alcohol (PVA) as a biocarrier for enhanced wastewater treatment: A comprehensive review', *Journal of Water Process Engineering*, 74, 107780. https://doi.org/10.1016/j.jwpe.2025.107780.

- Häyrynen, K., Langwaldt, J., Pongrácz, A., Väisänen, V., Mänttäri, M., and Keiski, R.L. (2008) 'Separation of nutrients from mine water by reverse osmosis for subsequent biological treatment', *Minerals Engineering*, 21(1), 2–9. https://doi.org/10.1016/j.mineng.2007.06.003.
- Huang, H., Yang, T., Lai, F., and Wu, G. (2017) 'Co-pyrolysis of sewage sludge and sawdust/rice straw for the production of biochar', *Journal of Analytical and Applied Pyrolysis*, 125, 61–68. https://doi.org/10.1016/j.jaap.2017.04.018.
- Huong, P.T., Jitae, K., Giang, B.L., Nguyen, T.D., and Thang, P.Q.(2019) 'Novel lanthanum-modified activated carbon derived from pine cone biomass as ecofriendly bio-sorbent for removal of phosphate and nitrate in wastewater', *Rendiconti Lincei*, 30(3), 637–647. https://doi.org/10.1007/s12210-019-00827-3.
- Issac, M., Dai, B. and Zhang, L. (2019) 'Kinetics underpinning the C-CO2 gasification of waste tyre char and its interaction with coal char upon co-gasification', *Fuel*, 256. https://doi.org/10.1016/j.fuel.2019.115991.
- Jamka, Z.N., Mohammed, W.T., Zhenjiang YOU, and Hussein Rasool Abid (2023) 'Enhancing Nitrate Ion Removal from Water using Fixed Bed Columns with Composite Chitosan-based Beads', *Iraqi Journal of Chemical and Petroleum Engineering*, 24(4), 75–81. Available at: https://doi.org/10.31699/ijcpe.2023.4.7.
- Jamka, Z.N. and Mohammed, W.T. (2023) 'Assessment of the Feasibility of Modified Chitosan Beads for the Adsorption of Nitrate from an Aqueous Solution', *Journal of Ecological Engineering*, 24(2), 265– 278. https://doi.org/10.12911/22998993/156886.
- Jeguirim, M., Belhachemi, M., Limousy, L., and Bennici, S. (2018) 'Adsorption/reduction of nitrogen dioxide on activated carbons: Textural properties versus surface chemistry A review', Chemical Engineering Journal. 493–504.: https://doi.org/10.1016/j.cej.2018.04.063.
- Kang, J. and Jeen, S.W. (2021) 'Simultaneous removal of nitrate and phosphate in groundwater using Ca-citrate complex', *Environmental Science and Pollution Research*, 28(27), pp. 35738–35750. https://doi.org/10.1007/s11356-021-13312-y.
- Khanday, W.A., Ahmed, M.J., Okoye, P.U., and Hummadi, E.H. (2025) 'Single-step H3PO4 activation of chitosan for efficient adsorption of amoxicillin and doxycycline antibiotic pollutants', *Inorganic Chemistry Communications*, 175, 114189.: https://doi.org/10.1016/j.inoche.2025.114189.
- Kizito, S., Wu, S., Wandera, S.M., Guo, L., and Dong, R. (2016) 'Evaluation of ammonium adsorption in biochar-fixed beds for treatment of anaerobically digested swine slurry: Experimental optimization and modeling', *Science of the Total Environment*, 563–564, 1095–1104.: https://doi.org/10.1016/j.scitotenv.2016.05.149.
- Konneh, M., Wandera, S.M., Murunga, S.I., and Raude, J.M. (2021) 'Adsorption and desorption of nutrients from abattoir wastewater: modelling and comparison of rice, coconut and coffee husk biochar', *Heliyon*, 7(11). https://doi.org/10.1016/j.heliyon.2021.e08458.
- Li, C., Xie, S., Wang, Y., Jiang, R., Wang, X., Lv, N., Pan, X., Cai, G., Yu, G., and Wang, Y. (2021) 'Multi-functional biochar preparation and heavy metal immobilization by co-pyrolysis of livestock feces and biomass waste', Waste Management, 134, 241–250. https://doi.org/10.1016/j.wasman.2021.08.023.
- Liu, X., Shen, F. and Qi, X. (2019) 'Adsorption recovery of phosphate from aqueous solution by CaO-biochar composites prepared from eggshell and rice straw', *Science of the Total Environment*, 666, 694–702. https://doi.org/10.1016/j.scitotenv.2019.02.227.
- Luo, X., Zhang, Z., Zhou, P., Liu, Y., Ma, G., and Lei, Z. (2015) 'Synergic adsorption of acid blue 80 and heavy metal ions (Cu2+/Ni2+) onto activated carbon and its mechanisms', *Journal of Industrial and Engineering Chemistry*, 27, 164–174. https://doi.org/10.1016/j.jiec.2014.12.031.
- Meng, M., Feng, Y., Zhang, M., Liu, Y., Ji, Y., Wang, J., Wu, Y., and Yan, Y. (2013) 'Highly efficient adsorption of salicylic acid from aqueous solution by wollastonite-based imprinted adsorbent: A fixed-bed column study', *Chemical Engineering Journal*, 225, 331–339. https://doi.org/10.1016/j.cej.2013.03.080.
- Mohamed, S. dhyaa and J. Ahmed, M. (2019) 'Enhanced conversion of Glycerol to Glycerol carbonate on modified Bio-Char from reed plant', *Iraqi Journal of Chemical and Petroleum Engineering*, 20(4), 15–20.https://doi.org/10.31699/ijcpe.2019.4.3.

- Mohammed, W.T. and Rashid, S.A. (2012) 'Phosphorus removal from wastewater using oven-dried alum sludge', *International Journal of Chemical Engineering* [Preprint]. https://doi.org/10.1155/2012/125296.
- Nguyen, C.T., Tungtakanpoung, D., Tra, V.T., and Kajitvichyanukul, P. (2022) 'Kinetic, isotherm and mechanism in paraquat removal by adsorption process using corn cob biochar produced from different pyrolysis conditions', Case Studies in Chemical and Environmental Engineering, 6. https://doi.org/10.1016/j.cscee.2022.100248.
- Olgun, A., Atar, N. and Wang, S. (2013) 'Batch and column studies of phosphate and nitrate adsorption on waste solids containing boron impurity', *Chemical Engineering Journal*, 222, 108–119. https://doi.org/10.1016/j.cej.2013.02.029.
- Priya, E., Kumar, S., Verma, C., Sarkar, S., and Maji, P.K. (2022) 'A comprehensive review on technological advances of adsorption for removing nitrate and phosphate from waste water', *Journal of Water Process Engineering*. https://doi.org/10.1016/j.jwpe.2022.103159.
- Ramani, B., Anjum, A., Bramer, E., Dierkes, W.K., Blume, A., and Brem, G. (2025) 'A comprehensive study on the effect of the pyrolysis temperature on the products of the flash pyrolysis of waste tires', *Journal of Environmental Chemical Engineering*, 13(2). https://doi.org/10.1016/j.jece.2025.115468.
- Raza, M. and Abu-Jdayil, B. (2023) 'Synergic interactions, kinetic and thermodynamic analyses of date palm seeds and cashew shell waste co-pyrolysis using Coats–Redfern method', Case Studies in Thermal Engineering, 47. https://doi.org/10.1016/j.csite.2023.103118.
- Salgot, M. and Folch, M. (2018) Wastewater treatment and water reuse', Current Opinion in Environmental Science and Health. 64–74. https://doi.org/10.1016/j.coesh.2018.03.005.
- Santos, M.S.N., Wancura, J.H.C., Oro, C.E.D., Vezaro, F.D., Ody, L.P., Tres, M.V., Zabot, G.L (2025) 'Urban agriculture and water recycling: A comprehensive outlook on current panorama', *Environmental Development*, 54, 101156. https://doi.org/10.1016/j.envdev.2025.101156.
- Singh Yadav, S.P., Wancura, J.H.C., Oro, C.E.D., Vezaro, F.D., Ody, L.P., Tres, M.V., and Zabot, G.L. (2023) 'Biochar application: A sustainable approach to improve soil health', *Journal of Agriculture* and Food Research. https://doi.org/10.1016/j.jafr.2023.100498.
- Thomas, H.C. and HENRY THOMAS Vol, B.C. (no date) *Heterogeneous Ion Exchange in a Flowing System*.
- Uludag-Demirer, S. and Othman, M. (2009) 'Removal of ammonium and phosphate from the supernatant of anaerobically digested waste activated sludge by chemical precipitation', *Bioresource Technology*, 100(13), 3236–3244. https://doi.org/10.1016/j.biortech.2009.02.030.
- Varela, C.F., Moreno-Aldana, L.C. and Agámez-Pertuz, Y.Y. (2024) 'Adsorption of pharmaceutical pollutants on ZnCl2-activated biochar from corn cob: Efficiency, selectivity and mechanism', *Journal of Bioresources and Bioproducts*, 9(1), 58–73. https://doi.org/10.1016/j.jobab.2023.10.003.
- Vijayaraghavan, K. and Balasubramanian, R. (2021) 'Application of pinewood waste-derived biochar for the removal of nitrate and phosphate from single and binary solutions', *Chemosphere*, 278. https://doi.org/10.1016/j.chemosphere.2021.130361.
- Wang, J., Amano, Y. and Machida, M. (2024) 'Nitrate removal from aqueous solution by glucose-based carbonaceous adsorbent: Batch and fixed-bed column adsorption studies', *Colloids and Surfaces A: Physicochemical and Engineering Aspects*, 686. https://doi.org/10.1016/j.colsurfa.2024.133296.
- Wang, J.P., Chen, Y.Z., Wang, Y., Yuan, S., and Yu, H., (2011) 'Optimization of the coagulation-flocculation process for pulp mill wastewater treatment using a combination of uniform design and response surface methodology', *Water Research*, 45(17), 5633–5640. https://doi.org/10.1016/j.watres.2011.08.023.
- Wang, Z., Burre, K.G., Zhang, M., Li, X., Policella, M., Lei, T., and Gupta, A.K. (2020) 'Co-pyrolysis of waste tire and pine bark for syngas and char production', *Fuel*, 274. https://doi.org/10.1016/j.fuel.2020.117878.
- Yang, J., Li, H., Zhang, D., We, M. and Pan, B. (2017) 'Limited role of biochars in nitrogen fixation through nitrate adsorption', *Science* of the Total Environment, 592, pp. 758–765. https://doi.org/10.1016/j.scitotenv.2016.10.182.

Yin, Q., Liu, M. and Ren, H. (2019) 'Biochar produced from the copyrolysis of sewage sludge and walnut shell for ammonium and phosphate adsorption from water', *Journal of Environmental Management*, 249.

https://doi.org/10.1016/j.jenvman.2019.109410.

Yoon, Y.H.E.E., and Nelson, J.H. (1984) 'Application of Gas Adsorption Kinetics I. A Theoretical Model for Respirator Cartridge Service Life', American Industrial Hygiene Association Journal, 45(8), 509– 516. https://doi.org/10.1080/15298668491400197. Zhang, J., Jin, J., Wang, M., Naidu, R., Liu, Y., Man, Y.B., Liang, X., Wong, M.H., Christie, P., Zhang, Y., Song, C., and Shan, S. (2020) 'Co-pyrolysis of sewage sludge and rice husk/ bamboo sawdust for biochar with high aromaticity and low metal mobility', Environmental Research, 191, 110034. https://doi.org/10.1016/j.envres.2020.110034



© 2026. The Author(s). This article is an open access article distributed under the terms and conditions of the Creative Commons Attribution-ShareAlike 4.0 (CC BY-SA) International License (http://creativecommons.org/licenses/by-sa/4.0/)